Applied Energy 162 (2016) 589–600

Contents lists available at ScienceDirect

Applied Energy

journal homepage: www.elsevier.com/locate/apenergy

Modelling study, efficiency analysis and optimisation of large-scale Adiabatic Compressed Air Energy Storage systems with low-temperature thermal storage

Xing Luo [a], Jihong Wang [a,c,*], Christopher Krupke [a], Yue Wang [a], Yong Sheng [b], Jian Li [c], Yujie Xu [b], Dan Wang [c], Shihong Miao [c], Haisheng Chen [b]

[a] School of Engineering, University of Warwick, UK
[b] Institute of Engineering Thermophysics, Chinese Academy of Sciences, China
[c] School of Electrical & Electronic Engineering, Huazhong University of Science & Technology, China

HIGHLIGHTS

- The paper presents an A-CAES system thermodynamic model with low temperature thermal energy storage integration.
- The initial parameter value ranges for A-CAES system simulation are identified from the study of a CAES plant in operation.
- The strategies of system efficiency improvement are investigated via a parametric study with a sensitivity analysis.
- Various system configurations are discussed for analysing the efficiency improvement potentials.

ARTICLE INFO

Article history:
Received 6 August 2015
Received in revised form 10 October 2015
Accepted 12 October 2015
Available online 11 November 2015

Keywords:
Energy storage
Compressed Air Energy Storage
Mathematical modelling
Efficiency
Optimisation
Power systems

ABSTRACT

The key feature of Adiabatic Compressed Air Energy Storage (A-CAES) is the reuse of the heat generated from the air compression process at the stage of air expansion. This increases the complexity of the whole system since the heat exchange and thermal storage units must have the capacities and performance to match the air compression/expansion units. Thus it raises a strong demand in the whole system modelling and simulation tool for A-CAES system optimisation. The paper presents a new whole system mathematical model for A-CAES with simulation implementation and the model is developed with consideration of lowing capital cost of the system. The paper then focuses on the study of system efficiency improvement strategies via parametric analysis and system structure optimisation. The paper investigates how the system efficiency is affected by the system component performance and parameters. From the study, the key parameters are identified, which give dominant influences in improving the system efficiency. The study is extended onto optimal system configuration and the recommendations are made for achieving higher efficiency, which provides a useful guidance for A-CAES system design.

1. Introduction

Power network reliability is facing a great challenge in coping with the rapid increase of intermittent renewable energy integration. To address the challenge, various solutions are studied, among which Electrical Energy Storage (EES) has been recognized as one of the enabling technologies in supporting the current and future grid operation [1–3]. Various EES technologies with a comprehensive characteristic matrix can offer technical and economic benefits from generation, transmission and distribution to demand side management [4]. Among all EES technologies, Compressed Air Energy Storage (CAES) shows its distinguished merits, such as large-scale, low cost, long lifetime and the established operation experience [4,5]. CAES is considered as one of the cheapest EES technologies in terms of capital cost ($/kW h) and maintenance cost ($/kW-year) [4–6]. CAES works in the process as: the ambient air is compressed via compressors into one or more storage reservoir(s) during the periods of low electricity demand (off-peak) and the energy is stored in the form of high pressure compressed air in the reservoir(s); during the periods of high electricity

* Corresponding author at: School of Engineering, University of Warwick, UK.
E-mail addresses: jihong.wang@warwick.ac.uk, jihongwang@hust.edu.cn (J. Wang).

http://dx.doi.org/10.1016/j.apenergy.2015.10.091
0306-2619/

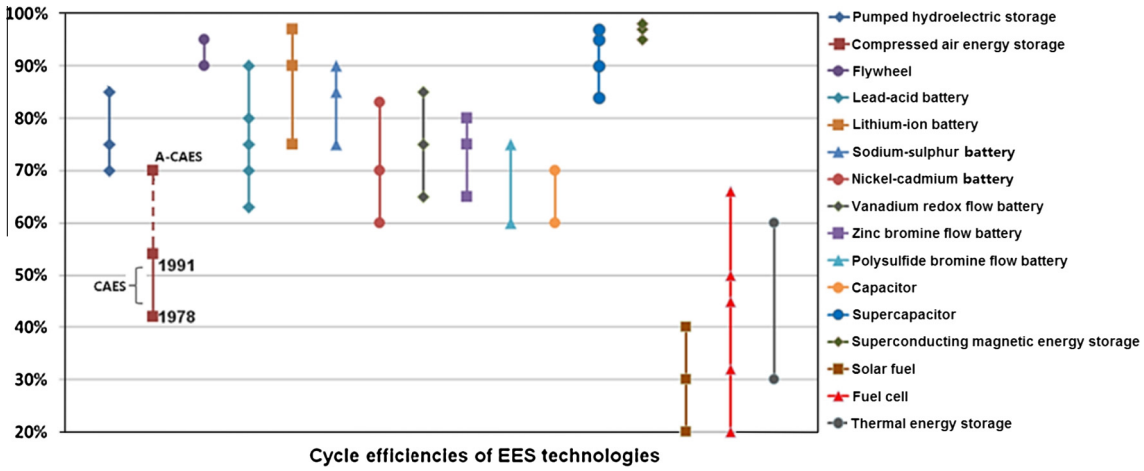

Fig. 1. Comparison of various EES technologies in cycle efficiencies [4].

demand (on-peak), the stored compressed air is released, heated by a heat source from the combustion of fossil fuels or other methods, and then the energy in compressed air (or post-combustion gas) is captured by turbines/expanders to generate electricity.

The major concern in deployment of CAES is its relatively low cycle efficiency compared with other EES technologies as shown in Fig. 1 [4,6,7]. There are two large-scale CAES plants in commercial operation worldwide, which are Huntorf CAES plant in Germany built in 1978 and McIntosh CAES plant in US built in 1991; both CAES plants burn gas as the heat source; the former has cycle efficiency around 42% and the latter is with around 53% cycle efficiency (Fig. 1) [4,8,9]. To improve CAES efficiency and avoid using fossil fuels, the Adiabatic CAES (A-CAES) system concept was proposed [8,10–13]. A-CAES combined with Thermal Energy Storage (TES) is to extract heat from the stage of air compression and store it in an adiabatic reservoir. The heat is then reused for the air expansion and electricity generation process. Fig. 2 illustrates a schematic layout for a typical A-CAES system, which is composed of: (i) a reversible motor/generator unit with clutch mechanisms to engage either with compressors or expanders; (ii) a multi-stage air compression unit operating with a group of Heat Exchangers (HEXs) to capture the heat produced; (iii) a multi-stage air expansion unit with another group of HEXs to heat the compressed air in the expansion stage; (iv) "hot" and "cold" thermal storage reservoirs working with the two groups of HEXs to form the TES cycle; (v) underground cavern(s) or aboveground tank(s) for storing compressed air; (vi) a power conditioning system for ensuring optimal generation of the electricity to match the requirements of the external power network; and (vii) a control system for coordinative operation of the whole system.

With the strategy of re-using the heat energy generated from air compression, A-CAES has a great potential to achieve a higher cycle efficiency compared to conventional CAES [4,10,14,15]. Currently, there mainly are two technology trends reported: A-CAES with high temperature TES and A-CAES with low temperature TES [10,12,16,14,15,17–20]. The research and development in this area has been very active in recent years. Pickard et al. presented an initial energy and exergy analysis of an ideal A-CAES system [21]. Zhang et al. studied the effect of TES on A-CAES system efficiency and the influences of temperature and pressure variations on the utilization of thermal energy from TES [22]. A hybrid EES system consisting of A-CAES and flywheel energy storage for wind power applications was proposed by Zhao et al. [16]. Following a thermodynamic analysis of A-CAES with artificial reservoirs, Grazzini and Milazzo designed a set of criteria for the A-CAES system with particular attention to HEXs [14]. Hartmann et al. contributed a simulation study of cycle efficiency on A-CAES systems, which shows the efficiency of a polytropic configuration is about 60% and the efficiency of an ideal isentropic configuration is about 70% [15]. Wolf and Budt recently proposed a low-temperature A-CAES design concept with the cycle efficiency in the range of 52–60%, and a brief economic analysis was also given in [17]. It is found that a number of A-CAES demonstration plants or facilities are under development or in early stage experiment around the world. A planned but currently paused large-scale A-CAES plant – ADELE in Germany was designed to have a capacity of 90 MW and 360 MW h with the target of ~70% cycle efficiency [4,10]. A 1.5 MW A-CAES demonstration facility located near Beijing, China, was recently built by the Institute of Engineering Thermophysics, Chinese Academy of Sciences, and its initial experimental tests are on-going [23]. LightSail Energy Ltd in US is developing the A-CAES system via using reversible reciprocating piston machines [24].

This paper examines the potential of system efficiency improvement for adopting low temperature TES in A-CAES. The main contributions of the paper are: (1) it presents a set of mathematical models of the system components and develops a whole system model of A-CAES with low temperature TES integration; (2) with the study of the Huntorf CAES plant, the range of a set of system parameters are identified to give the initial condition parameters in A-CAES system simulation study, which also provides a useful guideline for other researchers in selecting initial condition parameters; (3) with the simulation study using the whole system model, the optimal strategies for system efficiency improvements are investigated via a parametric study with sensitivity analysis of component parameters/performance indexes; and (4) following the achievements from the above study, the various system configurations aiming for system efficiency improvement are designed and discussed, and the recommendations are made.

2. Mathematical modelling of A-CAES systems

This section begins with the description of the system governing equations. Then the mathematical modelling to A-CAES system components is presented. The ideal air is assumed to be used in the whole modelling process.

2.1. Governing equations of modelling of A-CAES systems

In modelling all the system components, it is necessary to ensure the balance of the mass and energy flow in and out the

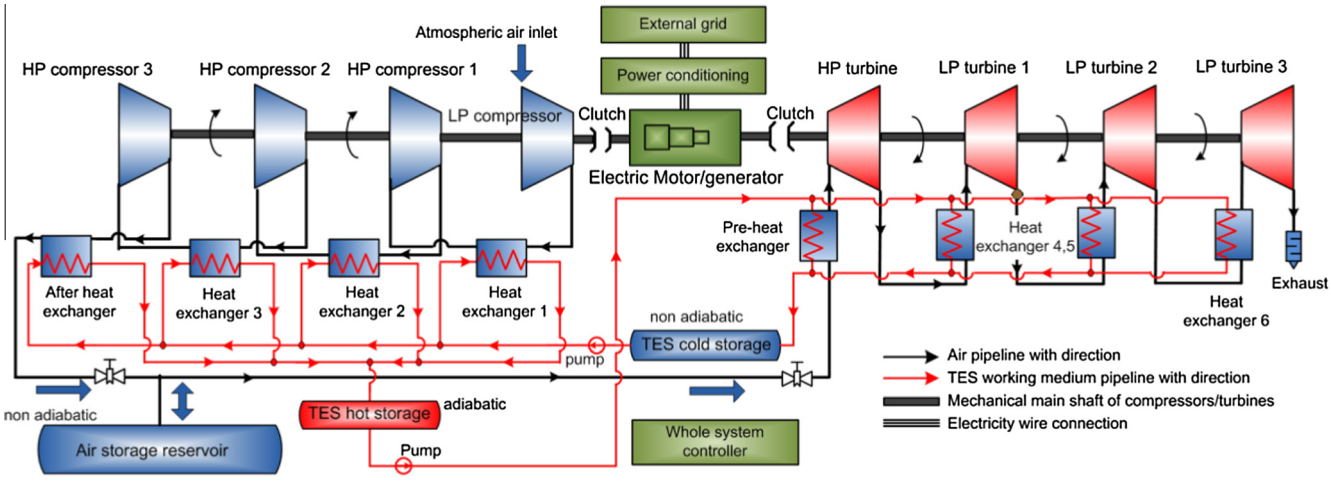

Fig. 2. Schematic diagram of an A-CAES plant/facility.

components. The following equations are the fundamental governing equations to modelling the whole system.

The rate of mass change to species j in a standard component which uses fluid as its working medium can be described [25,26],

$$\frac{dm_j}{dt} = \dot{m}_{\text{in},j} - \dot{m}_{\text{out},j} + N_j \tag{1}$$

where $\dot{m}_{\text{in},j}$ and $\dot{m}_{\text{out},j}$ stand for the mass flow rates of species j at the all inlets and outlets respectively; N_j represents the net production rate of species j by the chemical reaction(s); $\frac{dm_j}{dt}$ is also named the mass accumulation of species j. When there is no chemical reaction inside this component, N_j equals to zero [25,26].

When there is a steady flow of fluid in and out of a thermodynamic system (or component), from the first law of thermodynamics, the equation can be derived as ([26]),

$$\dot{m}_{\text{in}}\left(h_{\text{in}} + \frac{C_{\text{in}}^2}{2} + Z_{\text{in}}g\right) + \dot{Q} + \dot{W} = \dot{m}_{\text{out}}\left(h_{\text{out}} + \frac{C_{\text{out}}^2}{2} + Z_{\text{out}}g\right) \tag{2}$$

where the subscripts "in" and "out" represent the system inlet and outlet respectively; $\dot{Q}$ is the rate of change of heat transferred; $\dot{W}$ is the rate of change in energy transfer because of work done; h stands for the specific enthalpy of unit mass of the fluid; Z is the height above a datum level; Zg is the potential energy of unit mass of the fluid; C is the fluid velocity; $\frac{C^2}{2}$ is the kinetic energy of unit mass of the fluid. In theoretical calculation, it is normally assumed that $Z_{\text{in}} = Z_{\text{out}}$.

2.2. Modelling of compressors

From Fig. 2, the multi-stage air compression unit is formed by a group of Low Pressure (LP) and High Pressure (HP) compressors. Based on the mass balance of the compression process, the input mass flow rate of the compressors equals to the corresponding output mass flow rate at its steady state. Based on the properties of incoming flow and a given outlet pressure, the isentropic compression approach has been adopted to calculate the ideal mechanical power consumption. Then an isentropic efficiency has been considered in the modelling to calibrate the ideal mechanical power to be close to the practical working conditions. The isentropic efficiency (η_s) is defined by,

$$\eta_s = \frac{h_{\text{out},s} - h_{\text{in}}}{h_{\text{out}} - h_{\text{in}}} \tag{3}$$

where $h_{\text{out},s}$ is the specific enthalpy of working medium at the outlet in the ideal isentropic change of state, while h_{out} is the specific enthalpy at the outlet in the actual change of state. h_{in} is the specific enthalpy at the inlet.

The ideal mechanical power consumption ($\dot{W}_{c,s}$) for compressing the fluid can be calculated by ([16,26]),

$$\dot{W}_{c,s} = \dot{m}_c \Delta h_{\text{in}\to\text{out},s} = \dot{m}_c \int_{T_{c,\text{in}}}^{T_{c,\text{out},s}} C_p dT \tag{4}$$

where $\dot{m}_c$ is the mass flow rate of the compressor; C_p is the specific heat capacity at a constant pressure to the fluid working medium; $T_{c,\text{in}}$ and $T_{c,\text{out},s}$ represent the compressor inlet temperature and the compressor outlet temperature in the ideal isentropic change of state; $\Delta h_{\text{in}\to\text{out},s}$ is the ideal enthalpy change from the inlet to the outlet of the compressor in the ideal isentropic change of state. If this enthalpy change is calculated as a function of pressure ratio, from the ideal gas law ($Pv^{\gamma} = const.$ and $Pv = RT$) and the isentropic compression characteristics, Eq. (5) can be derived ([15,26]),

$$\Delta h_{\text{in}\to\text{out},s} = \frac{\gamma}{\gamma - 1} RT_{\text{in}}\left[\left(\frac{P_{c,\text{out},s}}{P_{c,\text{in}}}\right)^{\frac{\gamma-1}{\gamma}} - 1\right] \tag{5}$$

where R is the universal gas constant; γ is specific heat ratio; $P_{c,\text{in}}$ and $P_{c,\text{out},s}$ represent the compressor inlet pressure and the compressor outlet pressure in the ideal isentropic change of state.

From the energy balance Eq. (2) and assuming $\dot{Q} = 0,\ Z_{\text{in}} = Z_{\text{out}},\ C_{\text{in}} = C_{\text{out}}$ ([26]), Eq. (4) can be simplified to the following equation in terms of compressing the air if the process in each compressor is considered over a limited temperature change ($\Delta T \approx 473$ K) and the dry air is used ([14,26–29]),

$$\dot{W}_{c,s} = \dot{m}_c(h_{\text{out},s} - h_{\text{in}}) \tag{6}$$

From Eqs. (3) and (6), the actual power consumed by the compressor can be calculated by,

$$\dot{W}_c = \dot{m}_c(h_{\text{out},s} - h_{\text{in}})/\eta_{s,c} \tag{7}$$

where $\eta_{s,c}$ is the isentropic efficiency to the compressor. Thus, the total actual mechanical power consumption used by compressors is,

$$\dot{W}_{c,\text{total}} = \sum_{j_c=1}^{c,\text{num}} \dot{W}_{c,j_c} \tag{8}$$

where $\dot{W}_{c,j_c}$ stands for the actual power consumption by compressor j_c; c,num is the number of the compressors. Applying the

isentropic compression concept, the temperature at the compressor outlet can be calculated by ([14,26,29]),

$$T_{c,\text{out}} \approx T_{c,\text{in}}\left\{1+\left[\left(\frac{P_{c,\text{out}}}{P_{c,\text{in}}}\right)^{\left(\frac{\gamma-1}{\gamma}\right)}-1\right]\Big/\eta_{s,c}\right\} \tag{9}$$

where $P_{c,\text{out}}$ represent the compressor outlet pressure.

2.3. Modelling of compressed air storage reservoirs

To the compressed air storage process, the inner wall of the air storage reservoir(s) has been chosen as the controlled volume boundary for thermodynamic process analysis. It is assumed that there is no air leakage through the wall, and the air storage process is considered to have a constant volume in this paper. Considering the engineering feasibility and the capital cost, the compressed air storage reservoir(s) is set to be non-adiabatic.

The mass balance to the air storage reservoir(s) is,

$$\frac{d\rho_{\text{st}}}{dt}=\begin{cases}\dot{m}_{\text{in,st}}/V_{\text{st}}=\dot{\rho}_{\text{in,st}}A_{\text{in,st}}C_{\text{in,st}}/V_{\text{st}} & \text{air compression process}\\ -\dot{m}_{\text{out,st}}/V_{\text{st}}=-\dot{\rho}_{\text{out,st}}A_{\text{out,st}}C_{\text{out,st}}/V_{\text{st}} & \text{air expansion process}\end{cases} \tag{10}$$

where ρ_{st} is the density of air inside the storage reservoir(s); V_{st} is the controlled volume of the storage reservoir(s); the subscripts "in, st" and "out, st" represent the incoming and the outgoing air flows of the storage reservoir(s); A is the cross sectional area of the flow pipe; C is the air flow velocity.

From the first law of thermodynamics and Eq. (2), the following equation holds:

$$\frac{d(mu)}{dt}=\dot{m}_{\text{in}}h_{\text{in}}-\dot{m}_{\text{out}}h_{\text{out}}+\dot{Q}+\dot{W} \tag{11}$$

where $\frac{d(mu)}{dt}$ is the rate of increase in internal energy of the air inside the storage cavern. For the energy balance of compressed air storage reservoir, $\dot{W}=0$. Thus Eq. (11) can be decreased as ([27,28]),

$$\frac{d(mu)}{dt}=\dot{m}_{\text{in,st}}h_{\text{in,st}}-\dot{m}_{\text{out,st}}h_{\text{out,st}}-\varsigma_{\text{st}}A_{\text{wall,st}}(T_{\text{st}}-T_{\text{wall,st}}) \tag{12}$$

where ς_{st} is the heat transfer coefficient between the stored air and the reservoir wall; $A_{\text{wall,st}}$ is the area of heat transfer between the reservoir wall and the stored air; T_{st} and $T_{\text{wall,st}}$ are the air temperature inside the reservoir and the cavern wall temperature. From the definition of enthalpy, we can have ([26,27]),

$$\frac{d(mu)}{dt}=\frac{d[m(h-PV/m)]}{dt}=\frac{d(mh)}{dt}-\dot{P}V-P\dot{V} \tag{13}$$

As the air storage is considered as a constant volume process, $\dot{V}_{\text{st}}=0$. From Eqs. (12) and (13), the following equation to the air storage reservoir can be derived,

$$\frac{d(m_{\text{st}}h_{\text{st}})}{dt}=\dot{P}_{\text{st}}V_{\text{st}}+\dot{m}_{\text{in,st}}h_{\text{in,st}}-\dot{m}_{\text{out,st}}h_{\text{out,st}}-\varsigma_{\text{st}}A_{\text{wall,st}}(T_{\text{st}}-T_{\text{wall,st}}) \tag{14}$$

Expanding the enthalpy to show its relationship with the concentration of air, the following equation can be obtained ([27,30,31]),

$$\begin{aligned}\frac{d(m_{\text{st}}h_{\text{st}})}{dt}&=\frac{d([X_{\text{air}}]V_{\text{st}}\hat{h}_{\text{st}})}{dt}\\&=[\dot{X}_{\text{air}}]V_{\text{st}}\hat{h}_{\text{st}}+\dot{V}_{\text{st}}[X_{\text{air}}]\hat{h}_{\text{st}}+n_{\text{st}}C_{p,\text{air,mol}}\dot{T}_{\text{st}}\end{aligned} \tag{15}$$

where the subscript "st" stands for the storage reservoir; $[X_{\text{air}}]$ is the molar volumetric concentration of air; n is the number of moles of air; $\hat{h}$ is the specific enthalpy of air on a molar basis; $C_{p,\text{air,mol}}$ is the specific heat of air on a molar basis. From Eqs. (14) and (15), considering $\dot{V}_{\text{st}}=0$, the change rate of the air pressure in the storage reservoir can be derived as,

$$\begin{aligned}\dot{P}_{\text{st}}=[\dot{X}_{\text{air}}]\hat{h}_{\text{st}}&+\frac{1}{V_{\text{st}}}(n_{\text{st}}C_{p,\text{air,mol}}\dot{T}_{\text{st}}-\dot{m}_{\text{in,st}}h_{\text{in,st}}+\dot{m}_{\text{out,st}}h_{\text{out,st}})\\&+\frac{\varsigma_{\text{st}}A_{\text{wall,st}}}{V_{\text{st}}}(T_{\text{st}}-T_{\text{wall,st}})\end{aligned} \tag{16}$$

In Eq. (16), the values of the heat transfer coefficient (ς_{st}) and the area of heat transfer ($A_{\text{wall,st}}$) are difficult to estimate [28]. If considering combining them together, the effective heat transfer coefficient can be defined as $\tau_{\text{st,eff}}=\frac{\varsigma_{\text{st}}A_{\text{wall,st}}}{V_{\text{st}}}$. From the ideal gas law and $\dot{V}_{\text{st}}=0$, the rate of change of air temperature in the storage reservoir can be obtained,

$$\dot{T}_{\text{st}}=\frac{1}{m_{\text{st}}R}(M_{\text{air}}\dot{P}_{\text{st}}V_{\text{st}}-\dot{m}_{\text{st}}P_{\text{st}}T_{\text{st}}) \tag{17}$$

where M_{air} stands for the molar mass of air.

Considering the processes of air compression and air expansion happening at different time periods, the mass balance related to the incoming and the outgoing air flows of the storage reservoir (s) need to be considered,

$$\dot{m}_{\text{in,st}}t_{\text{charging}}=\dot{m}_{\text{out,st}}t_{\text{discharging}} \tag{18}$$

where t_{charging} and $t_{\text{discharging}}$ stand for the charging time of A-CAES (i.e., the time of air compression) and the discharging time of A-CAES (i.e., the time of air expansion). The charging–discharging time ratio equals to $t_{\text{charging}}/t_{\text{discharging}}$.

2.4. Modelling of turbines

Multi-stage air expansion unit in an A-CAES system consists of a group of HP and LP turbines (Fig. 2) and there is no fossil fuel combustion in the A-CAES air expansion process. With pressure decreasing of the incoming flow, the turbines release the compressed air energy to produce mechanical power. For the isentropic expansion method, with a given outlet pressure, the turbine module determines the thermodynamic state of the outgoing flow and the produced power. Similar to modelling of compressor, the turbine isentropic efficiency is also considered. For mass balance, the input mass flow rate of each turbine equals to the corresponding output mass flow rate, i.e., $\dot{m}_{t,\text{in}}=\dot{m}_{t,\text{out}}$.

The ideal mechanical power produced ($\dot{W}_{t,s}$), the actual mechanical power produced ($\dot{W}_t$) and the total actual power produced ($\dot{W}_{t,\text{total}}$) are described below,

$$\dot{W}_{t,s}=\dot{m}_t(h_{\text{in}}-h_{\text{out},s}) \tag{19}$$

$$\dot{W}_t=\eta_{s,t}\dot{m}_t(h_{\text{in}}-h_{\text{out},s}) \tag{20}$$

$$\dot{W}_{t,\text{total}}=\sum_{j_t=1}^{t,\text{num}}\dot{W}_{t,j_t} \tag{21}$$

where $\eta_{s,t}$ is the isentropic efficiency of the turbine; $\dot{m}_t$ is the mass change rate inside the turbine, $\dot{m}_t=\dot{m}_{t,\text{in}}=\dot{m}_{t,\text{out}}$; $\dot{W}_{t,j_t}$ is the actual produced mechanical power by Turbine j_t. t,num is the number of the turbines.

2.5. Modelling of thermal energy storage process

The TES mainly including HEXs and heat storage reservoirs is a key section to an A-CAES system. Effective TES design and management can improve the whole system performance especially to enhance the thermal energy recovery and in turn to increase the whole system cycle efficiency. The heat transfer area in the design

of HEX should be adequately sized to ensure optimal heat energy extraction during air compression and maximum heat energy recovery during air expansion. With low temperature TES, water in liquid phase is chosen as the working medium in the TES for heat transfer, because of its high specific heat capacity bringing the ability of storing more heat energy within a low temperature range. In addition, the pressure drop caused by the HEXs need to be considered.

Considering lowing capital and maintenance costs, the "hot" heat storage reservoir is designed to be adiabatic while the "cold" heat storage reservoir is set to be non-adiabatic (Fig. 2). It is assumed that, the water state changes inside the two TES storage reservoirs are no any leakage; the temperature of the "cold" heat storage reservoir equals to the temperature of environment at the static state. The mass balance to the water streams of the two TES storage reservoirs is described by,

$$\dot{m}_{\mathrm{in,hot,total}} t_{\mathrm{charging}} = \dot{m}_{\mathrm{in,cold,total}} t_{\mathrm{discharging}} \tag{22}$$

where $\dot{m}_{\mathrm{in,hot,total}}$ and $\dot{m}_{\mathrm{in,cold,total}}$ stand for the total coming mass flow rates to the "hot" heat storage reservoir during the charging time and to the "cold" heat storage reservoir during the discharging time respectively.

The counter flow design has been chosen for the HEXs to gain optimised heat transfer between the streams of compressed air and water, because of its high capability to transfer the heat energy compared to the parallel flow design. To modelling of the heat transfer and the two media state change inside the HEXs, the Number of Transfer Units method has been used, which is described below.

From [15,29], the heat transfer of one HEX can be determined by its effectiveness (ε) which can be defined by,

$$\varepsilon = \frac{\dot{\bar{C}}|T_{\mathrm{out}} - T_{\mathrm{in}}|}{\dot{\bar{C}}_{\mathrm{min}}(T_{\mathrm{in,hot}} - T_{\mathrm{in,cold}})} \tag{23}$$

where $\dot{\bar{C}}$ is the thermal capacity rate of the flow with the mass flow rate $\dot{m}$ entering at T_{out} and exiting at T_{out}, $\dot{\bar{C}} = \dot{m}C_P$; $\dot{\bar{C}}_{\mathrm{min}}$ is the minimum among the thermal capacity rates of the two flows to the HEX, $\dot{\bar{C}}_{\mathrm{min}} = \min(\dot{m}_{\mathrm{flow1}}C_{P,\mathrm{flow1}}, \dot{m}_{\mathrm{flow2}}C_{P,\mathrm{flow2}})$; $T_{\mathrm{in,hot}}$ and $T_{\mathrm{in,cold}}$ are the temperatures of "hot" fluid input and "cold" fluid input to the HEX respectively.

For the ith stage of air compression (or air expansion) in the A-CAES system, the inlet temperature of compressor ($T_{c,\mathrm{in},i}$) (or turbine ($T_{t,\mathrm{in},i}$)) can be calculated by the outlet temperature of the $(i-1)$th stage of air compression ($T_{c,\mathrm{out},i-1}$) (or air expansion ($T_{t,\mathrm{out},i-1}$)) by the given effectiveness (ε) of the interposed $(i-1)$th HEX which is located between the ith stage and the $(i-1)$th stage of air compression (or air expansion). From Eq. (23), the below equation can be derived,

$$T_{c,\mathrm{in},i} = T_{c,\mathrm{out},i-1} - \varepsilon\frac{\dot{\bar{C}}_{\mathrm{min}}}{\dot{m}_{\mathrm{hex,air},i-1}C_{p,\mathrm{air}}}(T_{c,\mathrm{out},i-1} - T_{\mathrm{wt,cold},i-1}) \quad \text{air compression process} \tag{24}$$

$$T_{t,\mathrm{in},i} = T_{t,\mathrm{out},i-1} + \varepsilon\frac{\dot{\bar{C}}_{\mathrm{min}}}{\dot{m}_{\mathrm{hex,air},i-1}C_{p,\mathrm{air}}}(T_{\mathrm{wt,hot},i-1} - T_{t,\mathrm{out},i-1}) \quad \text{air expansion proexcess} \tag{25}$$

where $\dot{m}_{\mathrm{hex,air},i-1}$ is the air mass flow rate of the $(i-1)$th heat exchanger; $T_{\mathrm{wt,cold},i-1}$ is the temperature of cold water at the inlet of the $(i-1)$th heat exchanger in air compression; $T_{\mathrm{wt,hot},i-1}$ is the temperature of hot water at the inlet of the $(i-1)$th heat exchanger in air expansion.

If considering counter flow, the effectiveness (ε) can be described as ([29]),

$$\varepsilon = \frac{1 - \exp[-\mathrm{NTU}(1-\chi)]}{1 - \chi \times \exp[-\mathrm{NTU}(1-\chi)]} \tag{26}$$

where

$$\mathrm{NTU} = \frac{UA}{\dot{\bar{C}}_{\mathrm{min}}} \tag{27}$$

$$\chi = \frac{\dot{\bar{C}}_{\mathrm{min}}}{\dot{\bar{C}}_{\mathrm{max}}} \tag{28}$$

To Eq. (27), the number of heat transfer units (NTU) can be calculated by the unit overall thermal conductance (U) times the effective heat transfer area (A) divided by the minimum thermal capacity rate ($\dot{\bar{C}}_{\mathrm{min}}$). UA is the heat transfer rate between two flows of the heat exchanger. To Eq. (28), $\dot{\bar{C}}_{\mathrm{max}} = \max(\dot{m}_{\mathrm{flow1}}C_{P,\mathrm{flow1}}, \dot{m}_{\mathrm{flow2}}C_{P,\mathrm{flow2}})$, and when $\dot{\bar{C}}_{\mathrm{min}} = \dot{\bar{C}}_{\mathrm{max}}$, for counter flow, $\varepsilon = \frac{\mathrm{NTU}}{1+\mathrm{NTU}}$. The detail of the calculation of NTU is described in [14].

2.6. Modelling of mixers, splitters, water pumps and motor/generator units

The stream with a given working medium through a mixer satisfies the mass and energy balances assuming no energy exchange and losses. The relevant equations can be described as,

$$\sum_{j_m}^{\mathrm{mix,num}} \dot{m}_{\mathrm{mixer,in},j_m} = \dot{m}_{\mathrm{mixer,out}} \tag{29}$$

$$\sum_{j_m}^{\mathrm{mix,num}} \dot{m}_{\mathrm{mixer,in},j_m} h_{\mathrm{mixer,in},j_m} = \dot{m}_{\mathrm{mixer,out}} h_{\mathrm{mixer,out}} \tag{30}$$

where $\dot{m}_{\mathrm{mixer,in},i}$ and $\dot{m}_{\mathrm{mixer,out}}$ stand for the mass flow rate of the j_mth incoming anabranch of the mixer and the outgoing mass flow rate of the mixer respectively; $h_{\mathrm{mixer,in},j_m}$ and $h_{\mathrm{mixer,out}}$ represents the specific enthalpy of the j_mth incoming anabranch and the specific enthalpy of the outgoing flow of the mixer individually.

The splitter is used for splitting one stream into two or multi anabranches. The difference factor (λ) to the j_sth outlet of splitter can be defined as,

$$\lambda_{j_s} = \frac{\dot{m}_{\mathrm{splitter,out},j_s}}{\dot{m}_{\mathrm{splitter,in}}} \tag{31}$$

where $\dot{m}_{\mathrm{splitter,in}}$ and $\dot{m}_{\mathrm{splitter,out},j_s}$ are the mass flow rates of incoming stream and the j_sth outgoing anabranch of the mixer respectively. Assuming there is no energy exchange and losses during the splitting process, the below equations can be obtained,

$$\dot{m}_{\mathrm{splitter,in}} = \sum_{j_s}^{\mathrm{split,num}} \dot{m}_{\mathrm{splitter,out},j_s} = \dot{m}_{\mathrm{splitter,in}} \sum_{j_s}^{\mathrm{split,num}} \lambda_{j_s} \tag{32}$$

$$h_{\mathrm{splitter,out},j_s} = h_{\mathrm{splitter,in}} \tag{33}$$

where $h_{\mathrm{splitter,in}}$ and $h_{\mathrm{splitter,out},j_s}$ represent the specific enthalpy of the incoming stream and the specific enthalpy of the j_sth outgoing anabranch respectively.

Two water pumps have been used in the water flow route for increasing the water saturation temperature and keeping the water circulation (refer to Fig. 2). The pump power ($\dot{W}_p$) can be calculated as,

$$\dot{W}_p = \frac{\dot{m}_{\mathrm{pump}}(P_{\mathrm{pump,out}} - P_{\mathrm{pump,in}})}{\rho_{\mathrm{water}}\eta_{\mathrm{pump}}} \tag{34}$$

where $\dot{m}_{\text{pump}}$ is the mass flow rate of water via the pump; $P_{\text{pump,out}}, P_{\text{pump,in}}$ stand for water pressures at the inlet and outlet of pump respectively; ρ_{water} is the density of water; η_{pump} represents pump efficiency.

Choosing the constants for the electrical motor efficiency η_m and the electrical generator efficiency η_g, the consumed electricity power during the air compression ($\dot{W}_{\text{con,elec}}$) and the generated electricity power during the air expansion ($\dot{W}_{\text{gen,elec}}$) can be calculated as,

$$\dot{W}_{\text{con,elec}} = \frac{1}{\eta_m}\sum_{j_c=1}^{c,\text{num}} \dot{W}_{c,j_c} + \dot{W}_{p,\text{cold}} + \dot{W}_{p,\text{hot}} \tag{35}$$

$$\dot{W}_{\text{gen,elec}} = \eta_g \sum_{j_t=1}^{t,\text{num}} \dot{W}_{t,j_t} \tag{36}$$

where $\dot{W}_{p,\text{cold}}$ and $\dot{W}_{p,\text{hot}}$ are the consumed powers by the two pumps located at the outlets of the "cold" heat storage reservoir and the "hot" heat storage reservoir respectively (Fig. 2).

With all the subsystem models presented above, the overall A-CAES system mathematical model is built by integration of these models. Fig. 3 shows the block diagram of the whole A-CAES system model with implemented sub model equations. All the subsystems and whole system models are implemented in Matlab/Simulink and Simulink based Thermolib toolbox environment for the simulation study.

3. Optimisation study and efficiency analysis of an A-CAES system

The whole system optimisation starts from a study of the parameters and the associated performance of Huntorf CAES plant. This helps the initial parameter settings for the A-CAES system model described in Section 2.

3.1. Study of Huntorf CAES plant

Huntorf CAES plant has/had been providing comprehensive services to the local power network, including emergency reserve, peak shaving, load following, compensation of intermittent wind power generation in North Germany [8,11,28]. The plant employs two salt dome caverns to store compressed air and runs in a daily cycle with about eight hours for air compression and two hours of air expansion operation [6,8]. The plant has consistently shown excellent performance over 30 years with 99% starting reliability [4,8]. The overall configuration layout of the Huntorf CAES plant can be found in [32]. The important specifications of the Huntorf plant are listed in Table 1. Actual operating data to the power production and the air pressures inside the caverns during a single day was reported in [28,32]. The data could be different in the publications because the Huntorf plant had been reformed or updated after its commercial operation from 1978.

The study of the Huntorf test data reported in [28,32] revealed that a constant effective heat transfer coefficient assumption cannot be used as described in Eq. (16) to reproduce the observed cavern behaviours. The heat transfer of the cavern is affected by the flow velocity which links to the charging and discharging flow characteristics of the cavern, so it can be considered as a combination of a natural convection (the heat transfer in the absence of net flow into/out of the cavern) and a forced convection (the heat transfer induced by the incoming and outgoing air flows). Thus, the effective heat transfer coefficient ($\tau_{\text{st,eff}}$) can be described as ([28,32,33]),

$$\tau_{\text{st,eff}} = \tilde{a} + \tilde{b}\left|\dot{m}_{\text{in,st}} - \dot{m}_{\text{out,st}}\right|^{0.8} \tag{37}$$

where the constant terms $\tilde{a}$ and $\tilde{b}$ stand for the effective heat transfer coefficient caused by the natural convection and the forced convection respectively, $\tilde{a} = 0.2356$ and $\tilde{b} = 0.0149$ ([28]). Eq. (37) was validated by comparison to the Huntorf plant test data, as shown in [28]. Thus this approach is chosen and used in the modelling of the A-CAES system and it is assumed that the system employs underground salt dome caverns as compressed air storage reservoirs.

3.2. Parameter optimisation analysis of A-CAES systems

In this section, the study on the influences of parameter changes to the system performance and efficiencies is carried out. Heat energy recycle efficiency ($\eta_{\text{heat,recycle}}$) and cycle efficiency of the overall A-CAES system (η_{cycle}) are considered, which are defined below,

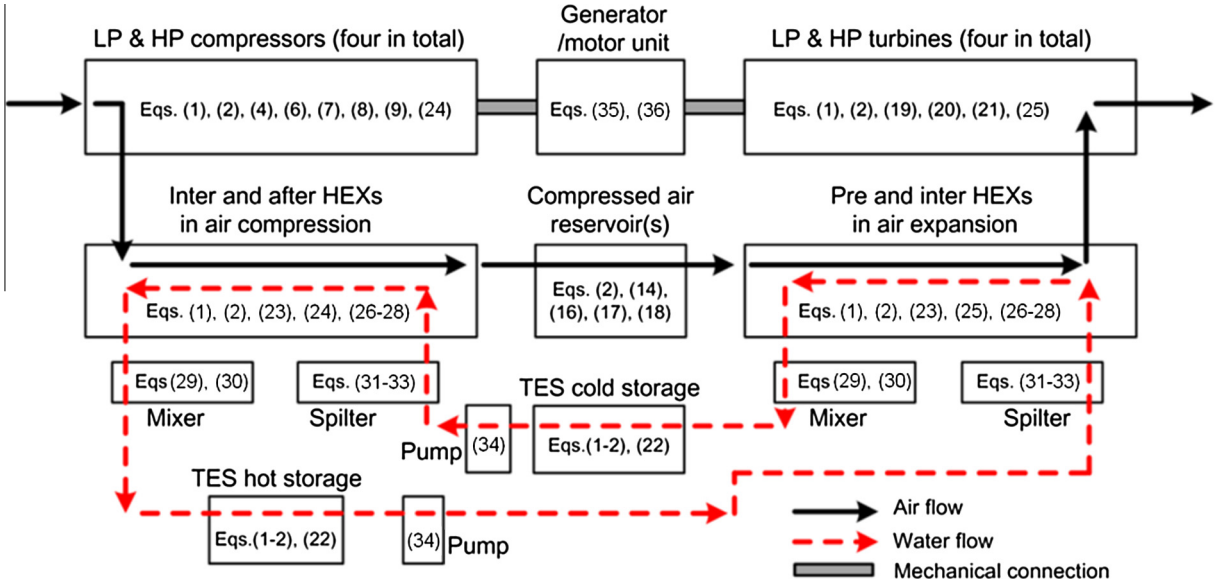

Fig. 3. Block diagram of the mathematical model of the whole A-CAES system.

Table 1
The specifications of the Huntorf plant for guiding the A-CAES system [4,8,28,32].

Specification item	Value	Unit
Low & high pressure compressors (series connection)		
Air flow rate of compressors	~108	kg/s
Rated power of the all compressors	60	MW
Air temperature at exit of after-cooler	~323	K
Maximum air pressure at exit of after-cooler	72	bar
Two underground salt dome storage caverns (parallel connection)		
Total cavern volume	~310,000	m^3
Cavern wall temperature	~313–323	K
Cavern operational pressure range	~43–66	bar
Maximum permissible cavern pressure	~70	bar
Maximum pressure reduction rate	~10–15	bar/h
High & low pressure gas turbines (series connection)		
Air flow rate of gas turbines	~417	kg/s
Rated power of the all gas turbines	290	MW
Inlet pressure of the high pressure turbine	~43	bar
Inlet pressure of the low pressure turbine	~8–11	bar
Charge–discharge time ratio of whole system	~4	/

$$\eta_{\text{heat,recycle}} = \frac{E_{\text{out,heat}}}{E_{\text{in,heat}}} = \frac{t_{\text{discharging}} \sum_{i_{\text{ex}}=1}^{\text{hex,ex,num}} \dot{W}_{\text{hex,ex},i_{\text{ex}}}}{t_{\text{charging}} \sum_{i_{\text{co}}=1}^{\text{hex,co,num}} \dot{W}_{\text{hex,co},i_{\text{co}}}} \tag{38}$$

$$\eta_{\text{cycle}} = \frac{E_{\text{out,elec}}}{E_{\text{in,elec}}} = \frac{t_{\text{discharging}} \eta_g \sum_{j_t=1}^{\text{t,num}} \dot{W}_{t,j_t}}{\left(\frac{1}{\eta_m} \sum_{j_c=1}^{\text{c,num}} \dot{W}_{c,j_c} + \dot{W}_{p,\text{cold}}\right) t_{\text{charging}} + \dot{W}_{p,\text{hot}} t_{\text{discharging}}} \tag{39}$$

where $E_{\text{in,heat}}$ and $E_{\text{out,heat}}$ represent the heat energy obtained from the air compression process and the heat energy provided to the air expansion process; $E_{\text{in,elec}}$, $E_{\text{out,elec}}$ stand for the whole system input electricity energy and the whole system output electricity energy; $\dot{W}_{\text{hex,co},i_{\text{co}}}$ is the rate of heat energy taken from the i_{co}th HEX in the compression process; $\dot{W}_{\text{hex,ex},i_{\text{ex}}}$ is the rate of heat energy extracted from the i_{ex}th HEX in the expansion process; the subscripts hex, co, num and hex, ex, num refer to the numbers of the HEXs in compression and expansion processes respectively.

Table 2 lists the base values of the parameters used in the A-CAES system model. Table 3 presents the selected parameters and their ranges of variations for conducting parametric study. With the whole A-CAES system configuration shown in Fig. 2, the simulation study for a number of parametric setting cases are performed, in which the cycle efficiency and the heat energy recycle efficiency were evaluated. Following the parametric study, a first-order sensitivity analysis was performed to analyse the impact of the parameters on the cycle efficiency of the overall system.

With the base values of parameters listed in Table 2, the simulation results show that, the overall system cycle efficiency is around 53.8% and the heat energy recycle efficiency is around 45.8%; the maximum air temperature at the outlet of the last compression stage is at 436 K and the lowest air temperature at the outlet of the last expansion stage is at 274 K; the water temperatures into the "hot" and "cold" storage reservoirs are at 382 K and 342 K respectively. These simulated results for temperatures are within the reasonable working ranges of the industrial facilities for air compression/expansion and TES with using liquid water as working medium [14,26,34,35]. However, it can be seen that the water temperature into the "cold" heat storage reservoir is higher compared to the ambient temperature and thus the stored heat energy from the "hot" heat storage reservoir has not been well utilized. This has become one of the challenges in development of A-CAES systems, which was encountered at the demonstration facility developed by the Institute of Engineering Thermophysics, Chinese Academy of Science. In the simulation study, it is assumed that the pressure ratios of the multi-stage air compression and expansion processes are evenly distributed for simplification. In practice, uneven distribution pressure ratios are normally used and this could lead to higher efficiency; some studies show that, if considering the A-CAES operating at a constant pressure, the even distribution pressure ratios could be approximately considered as the optimal pressure ratio at certain conditions ([34]).

Table 2
Base values of parameters of the A-CAES system model described in Section 2.

Parameters	Value	Unit
Ambient (environment) temperature	293.15	K
Ambient (environment) pressure	1.013	bar
Charge–discharge time ratio	2	/
Stage numbers of air compression & expansion	4 stages to the both	
High & low pressure air compressors (series connection)		
Rated power of the all compressors	~16.6	MW
Air flow rate of compressors	33	kg/s
Isentropic efficiency to compressors	80	%
Pressure ratio of each stage	2.75	/
High & low pressure air turbines (series connection)		
Rated power of the all air turbines	~17.8	MW
Air flow rate of air turbines	66	kg/s
Isentropic efficiency to air turbines	80	%
Expansion ratio of each stage	2.55	/
TES subsystem & cavern (heat exchangers parallel connection)		
Heat transfer rate of each HEX	80	kW/K
Water flow of each HEX in air compression	11	kg/s
Water flow of each HEX in air expansion	22	kg/s
Air pressure loss of heat exchanger	~1.5	%
Cavern wall temperature	~323	K
Maximum operational cavern pressure	~55	bar

Table 3
Optimal parameter study of the A-CAES system model described in Section 2.

No.	Parameters	Variation values	Variation range
(1)	Isentropic efficiency to each compressor	70–90%	±12.5%
(2)	Isentropic efficiency to each turbine	70–90%	±12.5%
(3)	Air flow rate of each compressor	20–46 kg/s	~ ±40%
(4)	Charge–discharge time ratio	1–3	±50.0%
(5)	Heat transfer rate of each HEX	40–120 kW/K	±50.0%
(6)	Water flow rate of HEX in air compression	5–17 kg/s	±55%
(7)	Cavern wall temperature	283–363 K	±12.5%
(8)	Air pressure loss of each HEX	0.5–2.5%	~ ±67%

As to the parameter optimisation analysis, the paper studies which the system key parameters are and how they influence the heat energy recycle efficiency and the cycle efficiency. Following the parameter ranges listed in Table 3, with the system configuration shown in Fig. 2, the simulation study is conducted and the simulation results are shown in Fig. 4. From Fig. 4(a) and (b), it can be seen that the higher isentropic efficiencies of air compressors and turbines are, the higher cycle efficiencies and heat energy recycle efficiencies will be achieved. The maximum permissible working air temperature to the compressor outlet is normally around 448–453 K [35]. As shown in Fig. 4(a), when the isentropic efficiency of the air compressor is reduced to around 72%, the air temperature at the last stage outlet reaches the maximum temperature boundary and the status of water to the "hot" heat storage reservoir gets into the saturation condition, that is, the water starts being transformed into vapour. The water status changes could result in difficulties to practical system operations. From the simulation results, the variations of isentropic efficiencies have more obvious influences on compressors, than air turbines. The performance (e.g., isentropic efficiency) of air compressors can directly

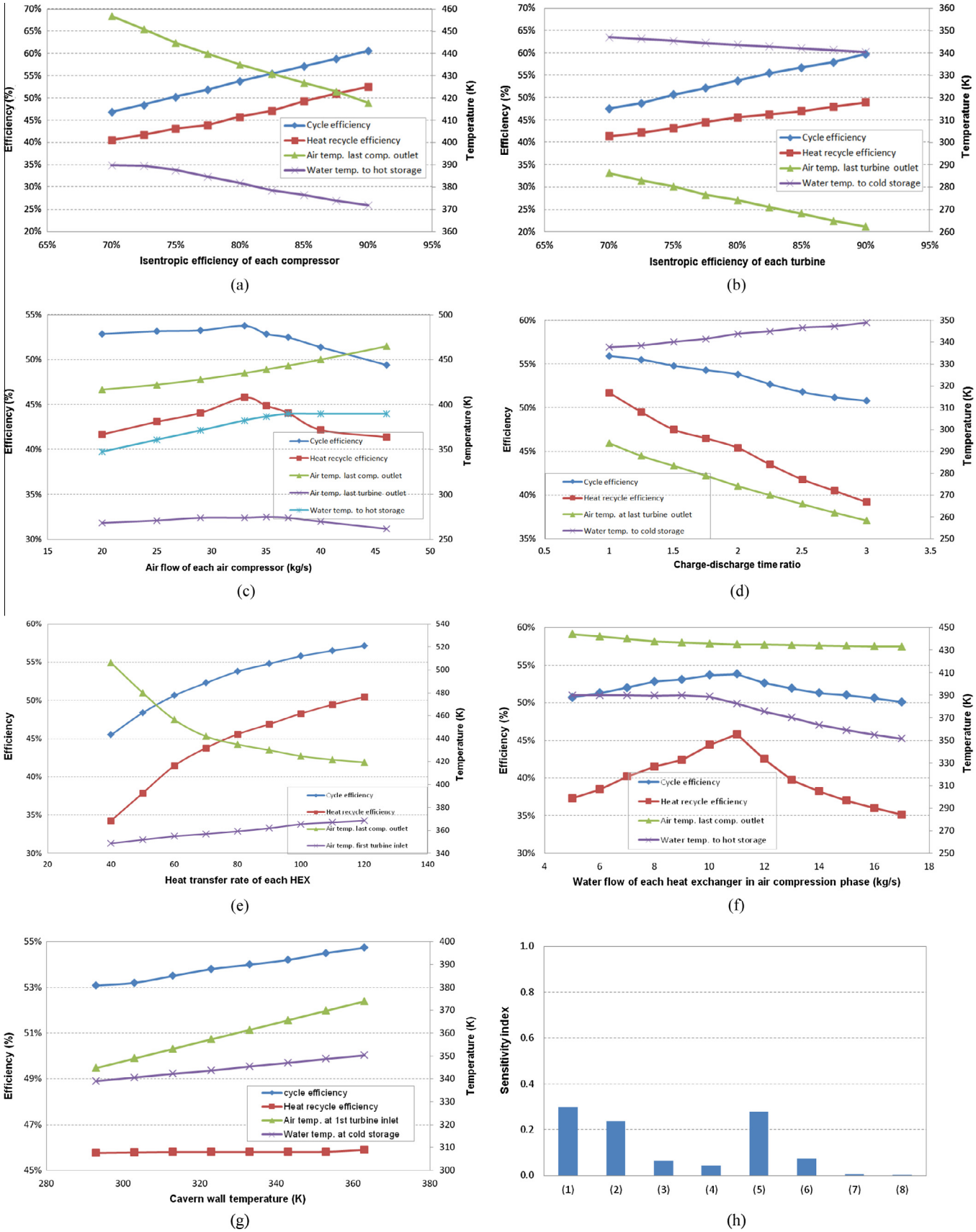

Fig. 4. Parametric study and sensitivity analysis of model parameters to the A-CAES system model.

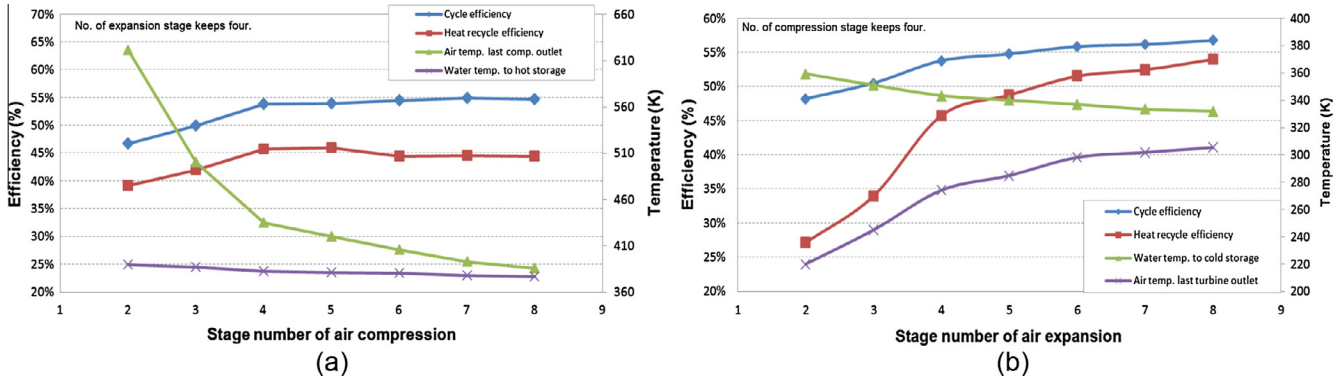

Fig. 5. A-CAES efficiencies as a function of air compression and expansion stage numbers.

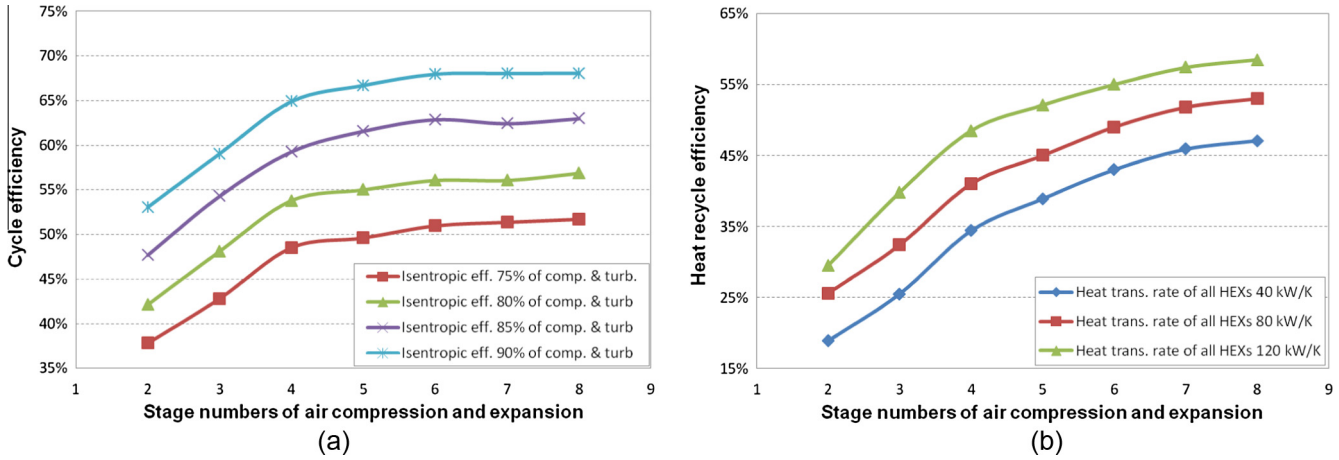

Fig. 6. A-CAES efficiencies as a function of both stage numbers of air compression & expansion (with different isentropic efficiencies of compressors/turbines and heat transfer rates of HEXs).

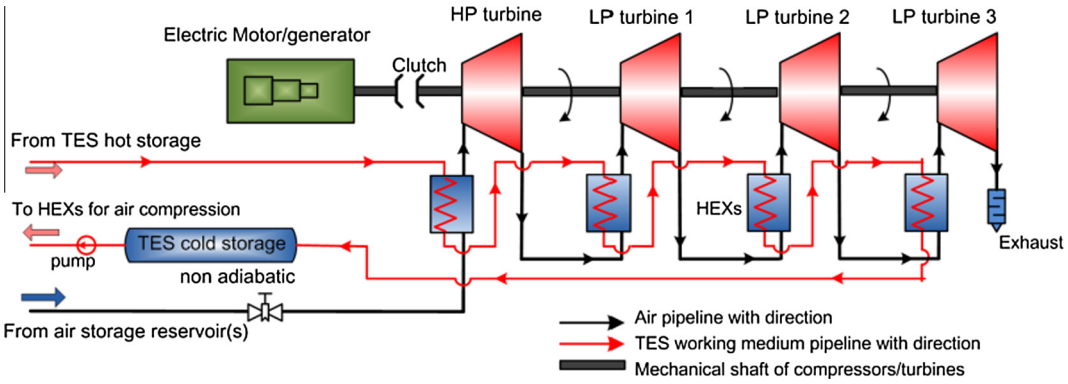

Fig. 7. Schematic diagram of an A-CAES air expansion with heat exchangers in series connection.

affect the adiabatic "hot" heat storage water temperature and, in turn, the stored "hot" heat energy. Due to the non-adiabatic "cold" heat storage receiver in use, the influence on the performance of air turbines is relatively small to the overall system.

The simulation results of the variation of the cycle efficiency and the heat energy recycle efficiency with respect to the air flow of each air compressor and the water flow of each HEX in air compression mode are shown in Fig. 4(c) and (f). Based on the mass balance of working mediums, both the air and water flows through the turbines and the HEXs in the air expansion process are varied. The peak values of the efficiencies are found in these two parametric setting cases (refer to Fig. 4(c) and (f)). The simulation results indicate the importance of parametric study to A-CAES.

Fig. 4(d) shows how the cycle efficiency and the heat energy recycle efficiency change as the charge–discharge time ratio varies. For instance, when the charge–discharge time ratio increases, assuming there is no change to the air and water flows through the compressors and the HEXs installed in the air compression system, air and water flow into the air expansion mode will also increase because of the mass balance of working mediums. In this situation, the two efficiencies decrease as shown in Fig. 4(d). It is

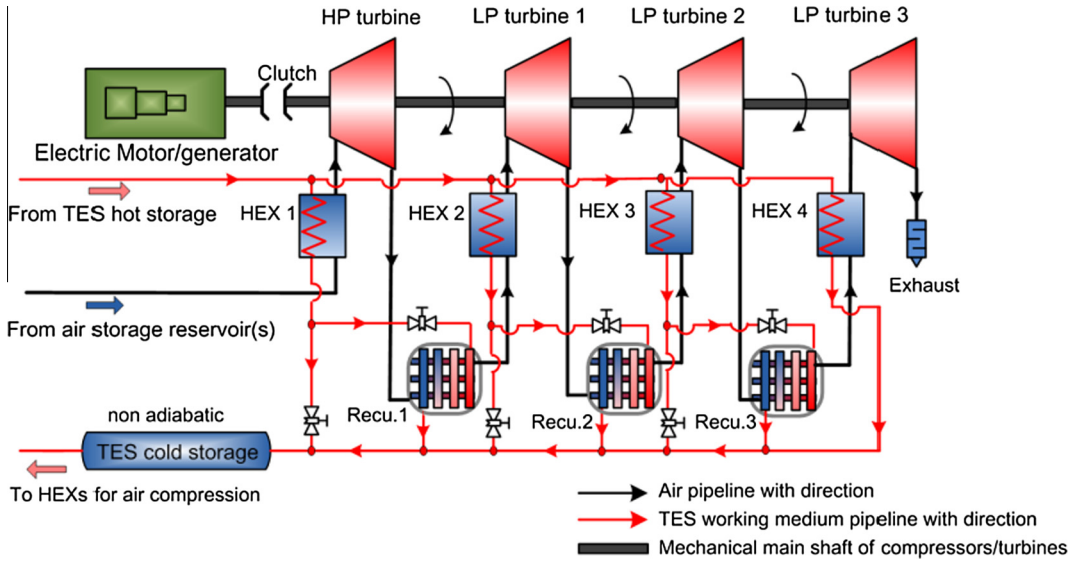

Fig. 8. Schematic diagram of an A-CAES air expansion with recuperators for exhaust heat recycle.

Table 4
An example of air compression process with pressure-based controlled air flow routes.

Air pressure inside the storage cavern	Description of the air flow route from ambient to the air reservoir
1 bar to ~2.75 bar	Six compressors in parallel connection to the whole air flow route
~2.75 bar to ~7.56 bar	Three sets of compressors in parallel (each set two compressors)
~7.56 bar to ~20.8 bar	Two sets of compressors in parallel (each set three compressors, Fig. 9)
~20.8 bar to ~57.2 bar	Six compressors in series connection to the whole air flow route

also noticed that, with the charge–discharge time ratio increase, sometime the air temperature at the last stage of expansion can decrease to around 260 K and even lower, which may bring difficulties in practice regarding air exhausting to the environment. From Fig. 4(c), (d) and (f), it can be seen that, if one parameter is adjusted, other system parameters needs to be adjusted according to the energy/mass balance and other fundamentals of thermodynamics. This is mainly due to the system sub process interactions and coupling with different components.

Fig. 4(e) illustrates the variation of the cycle and the heat energy recycle efficiencies while the heat transfer rate of each HEX varies. The heat transfer rate can heavily affect the performance of the HEXs, the heat energy extracted from air compression and the heat energy used in air expansion. From Fig. 4(e), it is seen that the heat energy recycle efficiency has been changed distinctly. It is also shown that, if the heat transfer rate of HEXs reduces to 60 kW/K or lower, the air temperature at the last stage compressor outlet will excess the normal allowed temperature boundary (around 448–453 K) [35]. This means that the normal system operation requirements cannot be met in this situation. From the simulation study, it is also found that the overall heat transfer effect from the HEXs in the air expansion process can regulate the water temperature into the "cold" heat storage reservoir. Therefore, improving the heat transfer effect of HEXs which are located in the air expansion process can achieve lowering water temperature into the "cold" heat storage reservoir and in turn to improve the system efficiencies.

Fig. 4(g) indicates the contribution from the cavern wall temperature to the overall system cycle efficiency and the heat energy recycle efficiency. In Fig. 4(a), although the air temperature at the 1st stage turbine (see HP turbine in Fig. 1) inlet increases distinctly, the efficiencies increased only by less than 2%. Similarly, from the simulation study, within a certain variation range of air pressure loss of each HEX (0.5–2.5%, Table 3), the cycle efficiency and the heat energy recycle efficiency also change mildly (less than 2%).

Among all cases under appropriate assumptions, it can be found that an increase in the isentropic efficiencies of air compressors/-turbines and the heat transfer rate of HEXs lead to a higher cycle efficiency and higher heat energy recycle efficiency obviously; an increase in the charge–discharge time ratio results in decreases of the efficiencies; there are the optimum values for the air flow of each compressor and the water flow of each HEX in air compression.

The definition of sensitivity analysis is described as "the study of how uncertainty in the output of a model can be apportioned to different sources of uncertainty in the model" [36,37]. The analysis approach used in the paper is a variance-based measurement, which has been used for the sensitivity analysis of simulation model for a long time and the method has been improved by Saltelli et al. [37]. There are a number of software tools developed for this, such as Simlab. The first-order sensitivity index $\widetilde{S}_i$ of parameters $\widetilde{X}_i$ on a generic model $\widetilde{Y}$, $\widetilde{Y} = f(\widetilde{X}_1, \widetilde{X}_2, \ldots, \widetilde{X}_k)$ can be defined as ([36,37]),

$$\widetilde{S}_i = \frac{V_{\widetilde{X}_i}(E_{\widetilde{X}_{\sim i}}(\widetilde{Y}|\widetilde{X}_i))}{V(\widetilde{Y})} \tag{40}$$

where $V(\widetilde{Y})(V(\widetilde{Y}) = \sigma^2_{\widetilde{Y}})$ indicates the variance of $\widetilde{Y}$; $V_{\widetilde{X}_i}(E_{\widetilde{X}_{\sim i}}(\widetilde{Y}|\widetilde{X}_i))$ represents the conditional variance, also named the first-order effect of $\widetilde{X}_i$ on $\widetilde{Y}$, $V_{\widetilde{X}_i}(E_{\widetilde{X}_{\sim i}}(\widetilde{Y}|\widetilde{X}_i)) \leqslant V(\widetilde{Y})$ and thus the value of sensitivity index $(\widetilde{S}_i)$ is in the range of 0–1. The details for sensitivity analysis can be found in [36,37]. Fig. 4(h) presents the sensitivity analysis results of cycle efficiency to the concerned system parameters. In Fig. 4(h), the sensitivities of concerned parameters are represented by their sensitivity indexes. A higher index value means a higher sensitiveness and higher importance of corresponding parameters to the cycle efficiency. From Fig. 4(h), the isentropic efficiencies of compressors/turbines and the heat transfer rate of HEXs are the most sensitive parameters in the A-CAES system model

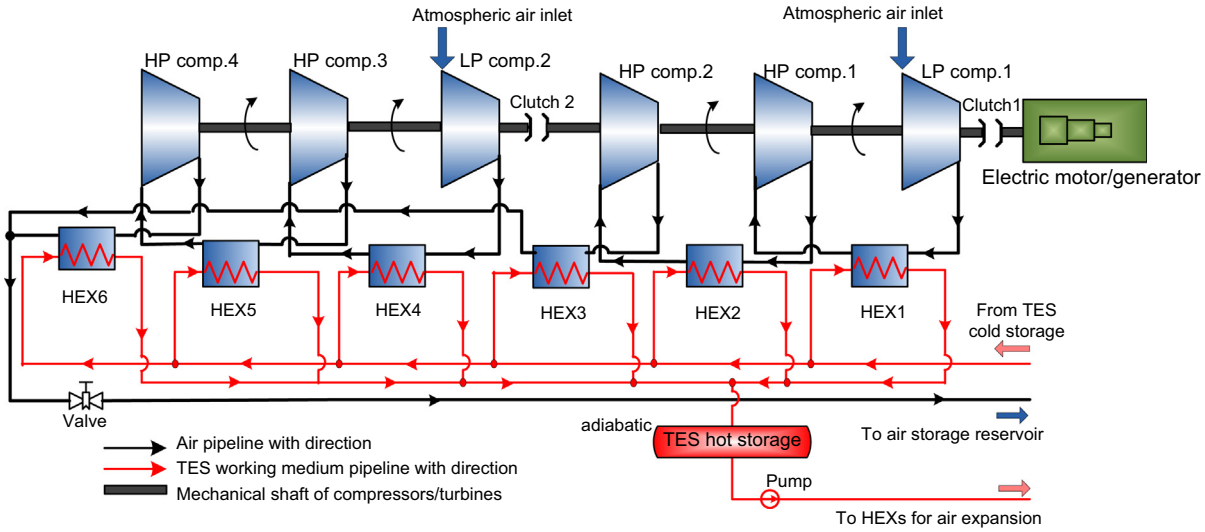

Fig. 9. Schematic diagram of an A-CAES air compression with two sets of compressors in parallel (each set having three compressors).

described in Section 2; the air/water flow rates and the charge–discharge time ratio show moderate sensitiveness; within a certain range the variations of the cavern wall temperature and the pressure loss of HEXs are less effective to the A-CAES system model.

3.3. Study of different A-CAES system configurations

This section presents the study on how different configurations of A-CAES systems contribute to the improvement of the system cycle efficiency and the heat energy recycle efficiency. From the study, increasing the numbers of air compression and expansion stages is an effective way for improving the efficiencies. Fig. 5 shows the simulation results of changing the numbers of air compression and expansion stages respectively. In this study, assuming the final compressed air pressure into the storage reservoir keeping constant, the compression ratio of compressors need to be modified based on the number of stages. To Fig. 5(a) and (b), the cycle efficiency increase to above 55%. In Fig. 5(b), the heat energy recycle efficiency can reach 54% and the water temperature into the "cold" heat storage reservoir can reduce to around 330 K. From the simulation study, fewer numbers of air compression and expansion stages mean harsh working conditions. For instance, if the number of stages of air compression changes to two or three, the air temperature at the last compressor outlet will exceed the maximum permissible temperature, 448–453 K (Fig. 5(a)).

From the above, the isentropic efficiencies of compressors/turbines and the heat transfer rate of HEXs can affect the system efficiencies distinctly. Fig. 6 presents the A-CAES efficiency as a function of both stage numbers of air compression and expansion with different isentropic efficiencies of compressors and turbines as well as heat transfer rates of the HEXs. The system cycle efficiency and the heat energy recycle efficiency can reach up to around 68% and 60% respectively. Thus, the system efficiencies studied in the paper can be much improved. From the simulation results, the water temperature into the "cold" storage can drop to around 325 K with eight stages of air compression and expansion and 120 kW/K heat transfer rate of HEXs. It should be mentioned that higher numbers of stages of air compression and expansion normally means more complexity of the whole system, which can affect the system reliability and stability in practice.

Based on the parametric study (Section 3.2), it can be seen that the water temperature into the "cold" heat storage reservoir is normally above 335 K and the available heat energy contained by water is lost. To improve the system efficiency, two new system configurations are analysed to explore possible solutions. Their schematic diagrams are shown in Figs. 7 and 8. For both of the system configurations, it is assumed that the layout and the associated working condition of air compression mode remain unchanged for all the analyses. Compared with the air expansion layout in Fig. 2, four HEXs in Fig. 7 are changed to series connection. Thus, the water flow rate via each HEX increases three times based on the mass balance principle of the working medium. The simulation study reveals that, with the values of parameters listed in Table 2, the water temperature into the "cold" heat storage reservoir increases by 1.4 K and the power output of all turbines decrease 0.11 MW. Thus, the system is less efficient. The key feature of the system configuration illustrated in Fig. 8 is to introduce extra recuperators on the by-passes of water flow routes to reuse the exhaust heat energy from the water loop. The by-pass starts from the HEX outlets and the recuperator heats the compressed air before it goes into the next stage HEX. The heat transfer rate of recuperators is assumed to be the same as that of HEXs. From the comparison of simulation results, the system configuration shown in Fig. 8 can reduce the water temperature into the cold storage by 1.6–6.0 K with consideration of the cases of one or multiple recuperators installed. The heat energy recycle efficiency and the cycle efficiency can be improved by around 6.6% and 2.6% separately. If a higher heat transfer rate of HEXs and recuperators (e.g. 120 kW/K) is chosen, the turbine's power output and the stored heat energy utilization will increase further. However, this configuration design will increase the capital cost as recuperators are adopted.

From the parametric study, it is concluded that the charging–discharging time ratio can affect the overall system efficiencies. Thus, to develop controllable air flow routes to A-CAES for varying charge/discharge time is a possible approach to improve the system efficiencies. For instance, to an initial air compression process, assuming that the compressed air pressure inside the cavern needs to increase from 1 to 57.2 bar and there are six compressors with even compression ratios of 2.75, Table 4 shows a compression process in this situation with the controllable air flow routes. Fig. 9 illustrates an A-CAES air compression mode with two sets of compressors in parallel (the 3rd sequence in Table 4). The whole process can be completed via controlled pneumatic valves. It can be seen that, by the approach of controlling air flow routes, the charging time of A-CAES can be varied compared to the system layout in

Fig. 2, which is caused by changes of the air flow rates from ambient to the compressed air storage reservoir. Correspondingly, the discharging time of air expansion can also be modified for improving system efficiency target.

4. Concluding remark

The paper presents the mathematical models of an A-CAES system components and developed a new whole system model of A-CAES with low temperature thermal storage. The model is implemented in Matab/Simulink software environment. With the system model developed in the paper, the system energy efficiency is analysed, especially, a comprehensive study is performed on how much the system parameter variations affect the system overall efficiency. From the analysis, it is found that the isentropic efficiencies of compressors and turbines and the heat transfer rates of HEXs are the key parameters to give the dominant influences on the system efficiency. In addition to system parameters, the system configuration can also lead to system efficiency improvement. From the study, multi-stage compression and expansion can improve system efficiency but it does not mean the system can have unlimited number of stages. Regulating the A-CAES charging time and discharging time via flow control can also lead to different system efficiencies. These are considered as the important factors for efficient system design in practice.

The results from optimal design study of low temperature A-CAES systems show that the system cycle efficiency and the heat energy recycle efficiency can potentially reach to around 68% and 60% respectively. The results confirm that the current relative low efficiency of CAES systems can be improved to address the main concern of CAES system design and deployment.

Acknowledgements

The authors would like to thank the research grant support from Engineering and Physical Sciences Research Council, UK (EP/K002228/1). Also, the authors want to give their thanks to the support from China National Basic Research Program 973 (2015CB251301) to enable the collaborative research between the UK and China researchers.

References

[1] Skea J, Nishioka S, Policies and practices for a low-carbon society. In: Strachan N, Foxon T, Fujino TJ, editors. Modelling long-term scenarios for low carbon societies. Climate Policy, vol. 8. UK: Taylor & Francis; 2008. p. 5–16.
[2] Beaudin M, Zareipour H, Schellenberglabe A, Rosehart W. Energy storage for mitigating the variability of renewable electricity sources: an updated review. Energy Sustain Dev 2010;14:302–14.
[3] Zhao H, Wu Q, Hu S, Xu H, Rasmussen CN. Review of energy storage system for wind power integration support. Appl Energy 2015;137:545–53.
[4] Luo X, Wang J, Dooner M, Clarke J. Overview of current development in electrical energy storage technologies and the application potential in power system operation. Appl Energy 2015;137:511–36.
[5] Technology roadmap: energy storage. Prepared by international energy agency (IEA). Technical report. Published 19 March 2014. <http://www.iea.org/publications/freepublications/publication/technology-roadmap-energy-storage-.html> [accessed 07.12.14].
[6] Chen H, Cong TN, Yang W, Tan C, Li Y, Ding Y. Progress in electrical energy storage system: a critical review. Prog Nat Sci 2009;19:291–312.
[7] Rastler D. Electricity energy storage technology options: a white paper primer on applications, costs, and options. Electric power research institute (EPRI). Technical report. Published December 2010.
[8] Succar S, Williams RH, editors. Compressed air energy storage: theory, resources, and applications for wind power. Princeton Environmental Institute. Energy Anal Group; 2008.
[9] Samir S. In: Levine JG, editor. Large energy storage systems handbook. CRC Press; 2011. p. 112–52.
[10] ADELE – adiabatic compressed air energy storage for electricity supply. RWE Power. Report. Published January 2010. <http://www.rwe.com/web/cms/mediablob/en/391748/data/364260/1/rwe-power-ag/innovations/Brochure-ADELE.pdf> [accessed 07.12.14].
[11] Succar S, Denkenberger DC, Williams RH. Optimization of specific rating for wind turbine arrays coupled to compressed air energy storage. Appl Energy 2012;96:222–34.
[12] Liu W, Li Q, Liang F, Liu L, Xu G, Yang Y. Performance analysis of a coal-fired external combustion compressed air energy storage system. Entropy 2014;16:5935–53.
[13] Nakhamkin M, Chiruvolu M, Daniel C. Available compressed air energy storage (CAES) plant concepts. In: The Proceedings of Power-Gen Conference, December 2007.
[14] Grazzini G, Milazzo A. A thermodynamic analysis of multistage adiabatic CAES. Proc IEEE 2012;100:461–72.
[15] Hartmann N, Vöhringer O, Kruck C, Eltrop L. Simulation and analysis of different adiabatic compressed air energy storage plant configurations. Appl Energy 2012;93:541–8.
[16] Zhao P, Dai Y, Wang J. Design and thermodynamic analysis of a hybrid energy storage system based on A-CAES (adiabatic compressed air energy storage) and FESS (flywheel energy storage system) for wind power application. Energy 2014;70:674–84.
[17] Wolf D, Budt M. LTA-CAES – a low-temperature approach to adiabatic compressed air energy storage. Appl Energy 2014;125:158–64.
[18] Dreißigacker V, Zunft S, Müller-Steinhagen H. A thermo-mechanical model of packed-bed storage and experimental validation. Appl Energy 2013;111:1120–5.
[19] Marquardt R, Zunft S, et al. AA-CAES – opportunities and challenges of advanced adiabatic compressed-air energy storage technology as a balancing tool in interconnected grids. In: Proceedings of 40 Kraftwerkstechnisches Kolloquium, Dresden, Germany, October 2008.
[20] Buffa F, Kemble S, Manfrida G, Milazzo A. Exergy and exergoeconomic model of a ground-based CAES plant for peak-load energy production. Energies 2013;6:1050–67.
[21] Pickard WF, Hansing NJ, Shen AQ. Can large-scale advanced-adiabatic compressed air energy storage be justified economically in an age of sustainable energy? J Renew Sustain Energy 2009;1:033102.
[22] Zhang Y, Yang K, Li X, Xu J. The thermodynamic effect of thermal energy storage on compressed air energy storage system. Renew Energy 2013;50:227–35.
[23] Advanced compressed air energy storage won the first prize of Beijing science and technology. n.d. <http://www.escn.com.cn/news/show-222217.html> [accessed 07.04.15].
[24] LightSail Energy Ltd. We store energy in compressed air. n.d. <http://www.lightsail.com/> [accessed 12.06.14].
[25] Department of civil & environmental engineering, Michigan Technological University. Mass and energy balances. n.d. <http://www.cee.mtu.edu/~reh/courses/ce251/251_notes_dir/node3.html> [accessed 12.04.15].
[26] Eastop TD, Mcconkey A. Applied thermodynamics for engineering technologists. 5th ed. New York, U.S.: Longman Scientific & Technical and John Wiley & Sons Inc; 1993.
[27] Luo X, Wang J, Sun H, Derby JW, Mangan SJ. Study of a new strategy for pneumatic actuator system energy efficiency improvement via the scroll expander technology. IEEE/ASME Trans Mechatronics 2013;18:1508–18.
[28] Raju M, Kumar Khaitan S. Modeling and simulation of compressed air storage in caverns: a case study of the Huntorf plant. Appl Energy 2012;89:474–81.
[29] Thermolib user manual: thermodynamic systems library, Release 5.2., Eutech Scientific Engineering GmbH, January 2013.
[30] Wang J, Luo X, Yang L, Shpanin LM, Jia N, Mangan S, et al. Mathematical modeling study of scroll air motors and energy efficiency analysis—Part II. IEEE/ASME Trans Mechatronics 2011;16:122–32.
[31] Luo X, Sun H, Wang J. An energy efficient pneumatic-electrical system and control strategy development. In: Proc. 2011 Am. Control Conf., IEEE; 2011. p. 4743–8.
[32] Crotogino F, Mohmeyer K, Scharf R. Huntorf CAES: more than 20 years of successful operation. In: Proc of SMRI spring meeting, Orlando, Florida, USA, 15–18, April 2001.
[33] Winterton RHS. Where did the Dittus and Boelter equation come from? Int J Heat Mass Transfer 1998;41:809–10.
[34] Guo H, Xu J, Chen H, Tan Q. Analysis of the efficiency of a AA-CAES system operating at a constant pressure. Chin J Eng Therm Energy Power 2013;28:540–6.
[35] Aftercoolers: why aftercoolering required? eCompressedair Ltd. n.d. <http://www.ecompressedair.com/library-pages/ aftercoolers.aspx> [accessed 07.02.15].
[36] Saltelli A, Tarantola S, Campolongo F, Ratto M. Sensitivity analysis in practice: a guide to assessing scientific models. John Wiley & Sons, Ltd.; 2004.
[37] Saltelli A, Ratto M, Andres T, Campolongo F, Cariboni J, Gatelli D, et al. Global sensitivity analysis. The primer. John & Sons Ltd.; 2008.